Planar Flow Casting of $Fe_{71}Si_{13.5}B_9Nb_3Cu_1Al_{1.5}Ge_1$ Ribbons

S. Sohrabi, H. Arabi, A. Beitollahi, and R. Gholamipour

In this study, the planar flow casting (PFC) technique for producing wide amorphous ribbons of $Fe_{71}Si_{13.5}B_9Nb_3Cu_1Al_{1.5}Ge_1$ alloy is investigated. Various ribbons of the mentioned alloy were produced through applying different values of wheel speed and ejection pressure. In addition, effects of wheel speed (13, 23, and 33 m/s) on the structure, degree of amorphicity, and surface quality of the ribbons were examined. The results showed that the trends of thickness variation with increasing wheel speed and ejection pressure for $Fe_{71}Si_{13.5}B_9Nb_3Cu_1Al_{1.5}Ge_1$ ribbons are in good agreement with what the Bernoulli equation in fluid dynamics predicts for the PFC process. Further, based on x-ray diffraction and differential scanning calorimeter results, it was shown that the degree of amorphicity increases by increasing the wheel speed. Besides, surface roughness measurements and scanning electron microscope micrographs of the ribbons revealed that the surface quality of the prepared ribbons improved by increasing the wheel speed.

1. Introduction

The planar flow casting (PFC) process, first reported by Narasimhan (Ref 1), is one of the most popular techniques among various rapid solidification processing (RSP) methods both in academic and industrial communities due to its capability to fabricate wide, thin, and continuous ribbons directly from the melt with amorphous or nanocrystalline microstructures. The process is used extensively for producing soft magnetic ribbons for transformer applications and foils for other applications such as soldering (Ref 2). In the PFC process, the metal is first melted in a crucible by an induction furnace and then is ejected onto a moving quenching wheel through a nozzle by applying a pressurized gas into the nozzle (Ref 3). The nozzle is so close to the wheel that the melt is constricted at the wheel-nozzle narrow gap and a melt puddle is formed as a result. Because of the wheel rotation, a thin metallic ribbon is then expelled from the melt puddle. Tkatch et al. (Ref 4) reported that due to large amounts of heat transfer at the wheel-melt interface, the melt undergoes extremely high cooling rates (between 10^4 and 10^7 K/s), leading to the

formation of amorphous phase (with no long-range atomic order) in the microstructure.

Geometry, uniformity, and surface quality of ribbons produced by the PFC process are controlled by cooling wheel speed (Vs), ejection pressure (P), nozzle slit breadth (d), wheel-nozzle gap distance (g), and the molten metal's temperature. Based on Bernoulli's equation in fluid dynamics (Ref 5), the dependence of ribbon thickness (t) on the above parameters is expressed as

$$t \propto \frac{d}{Vs}\left(\frac{2P}{\rho}\right)^{1/2} = K\frac{d}{Vs}\left(\frac{2P}{\rho}\right)^{1/2} \qquad \text{(Eq 1)}$$

where ρ is the density of the molten alloy and K is a coefficient representing simultaneous influence of the wheel-nozzle gap distance, nozzle slot breadth, and the melt superheat temperature (Ref 5).

A combination of mentioned parameters determines the surface quality of ribbons. High quality ribbons, having very smooth upper and lower surfaces, are produced when optimum amounts of the above parameters for a specific molten alloy are applied (Ref 6). Moreover, there are other kinds of patterns which usually appear on the ribbons' surfaces as a consequence of using unbalanced processing parameters. Praisner et al. (Ref 7) illustrated surface patterns of ribbons produced at different PFC processing conditions and suggested that applying low and high amounts of the molten metal's temperature causes the formation of dimpled and striated patterns, respectively, while processing of ribbons at low to moderate and high wheel speeds is characterized by wavy and herringbone (i.e., fine markings which are spaced very close to each other) patterns, respectively. Byrne et al. (Ref 8) analyzed that the wave-like pattern, which appears frequently over a wide range of processing conditions for various alloys (Ref 6, 7, 9), originates from the oscillations of the melt puddle at a natural frequency which is determined by the balance between liquid inertia and surface tension.

Melt puddle oscillations can capture the air which exists in the boundary layer of the roller and correspondingly, the

S. Sohrabi and A. Beitollahi, Center of Excellence for Advanced Materials and Processing (CEAMP), School of Metallurgy and Materials Engineering, Iran University of Science and Technology (IUST), Narmak, 1684613114 Tehran, Iran; H. Arabi, Center of Excellence for High Strength Alloys Technology (CEHSAT), School of Metallurgy and Materials Engineering, Iran University of Science and Technology (IUST), Narmak, 1684613114 Tehran, Iran; and R. Gholamipour, Iranian Research Organization for Science and Technology (IROST), Forsat, 158153538 Tehran, Iran. Contact e-mail: sajadsohrabi@metaleng.iust.ac.ir.

ribbon's surface quality is further aggravated by the formation of peaks and troughs on the wheel side surface of the ribbon (Ref 8, 10). These anomalies influence the local thermal conditions and may adversely affect the cooling rate of the molten alloy during melt spinning.

Nanocrystalline soft magnetic alloys of nominal $Fe_{73.5}Si_{13.5}B_9Nb_3Cu_1$ composition, known as FINEMET alloy, were innovated by Yoshizawa et al. (Ref 11). In their work, amorphous ribbons of the above composition were fabricated using the single roller melt spinning technique and then subjected to a specific heat treatment cycle to obtain a nanocrystalline structure. A homogeneous α-Fe(Si) single phase was formed with the average grain size of 10-15 nm dispersed in an amorphous matrix. These alloys possess superior soft magnetic properties such as high saturation induction and magnetic permeability and low coercivity to routine soft magnetic alloys. Several attempts have been made to optimize magnetic properties of FINEMET-type alloys by modifying the conventional nominal composition. Shahri et al. (Ref 12) investigated rapidly solidified FINEMET ($Fe_{73.5}Si_{13.5}B_9Nb_3Cu_1$) ribbons without and with partial substitutions of Al (1.5 at.%) and Ge (1 at.%) elements and observed an ultrasoft magnetic behavior for FINEMET alloys when Al and Ge elements were added to the conventional nominal composition.

The present study examines a fabrication technique of wide amorphous ribbons of $Fe_{71}Si_{13.5}B_9Nb_3Cu_1Al_{1.5}Ge_1$ alloy by the PFC process. In this regard, dependence of the thickness variations upon the wheel speed and applied pressure and also the effect of the wheel speed on the degree of amorphicity and surface quality of produced ribbons are investigated.

2. Experimental Procedure

The stoichiometric composition of the alloy used in this study was $Fe_{71}Si_{13.5}B_9Nb_3Cu_1Al_{1.5}Ge_1$ (at.%). 5-mm-wide ribbons of the alloy were fabricated using a single roller melt spinning apparatus operating in the air. For each casting run, a 10 g bar charge of the alloy was prepared using a laboratory-scale vacuum arc remelting (VAR) furnace. The charge was then placed into an alumina crucible and melted by a 20 kW induction furnace. Subsequently, the molten alloy was ejected through the nozzle by supplying a high purity argon gas to the crucible onto a 25-cm diameter rotating Cu wheel. The nozzle

was in the form of a rectangular slit with a length of 5 mm and breadth of 0.4 mm. The casting runs were performed by applying wheel speeds of 13, 18, 23, 28, and 33 m/s (keeping the wheel-nozzle gap at 0.2 mm and ejection pressure at 20 kPa) and ejection pressures of 10, 20, and 30 kPa (keeping the wheel-nozzle gap at 0.2 mm and wheel speed at 23 m/s). During all PFC runs, the superheat temperature was controlled by the furnace feedback system.

Structural characterization of ribbons produced at wheel speeds of 13, 23, and 33 m/s was carried out by the x-ray diffraction (XRD) technique using Cu-$K_{\alpha 1}$ radiation. Thermal stability of the as-spun ribbons, produced at wheel speeds of 13, 23, and 33 m/s, was examined using a METTLER differential scanning calorimeter (DSC) under ultrapure argon (99.9999%) atmosphere at a 20 K/min heating rate.

A TIME-TR200 surface roughness tester device was utilized to measure the surface roughness of both the contact (wheel) and free sides of the ribbons produced at wheel speeds of 13, 23, and 33 m/s. The device was operated laterally at a tracing length of 5 mm and cutoff length of 0.8 mm. An arithmetic average (R_a) value was used as a measure of the surface roughness. Scanning electron microscope (SEM) micrographs were also used to examine contact side of the ribbons.

3. Results and Discussion

3.1 Thickness Variation

Figure 1 shows the variation of thickness with increasing the wheel speed (Vs) and ejection pressure (P). Curves fitted by a power regression with least squares (R^2) of 0.984 and 0.998 reveal that $t \propto Vs^{-1.08}$ and $t \propto P^{0.514}$, respectively. Furthermore, Eq 1 which is taken from Bernoulli's momentum balance equation for the PFC process prognosticates that $t \propto Vs^{-1}$ and $t \propto P^{0.5}$. Accordingly, the experimental data obtained in this research are highly in line with what Bernoulli's theory anticipates for the dependence of thickness on the Vs and P during the PFC process.

3.2 Dependence of Structure and Degree of Amorphicity of Ribbons on the Wheel Speed

Figure 2 represents XRD multiplot patterns for the contact and free sides of ribbons produced at different wheel speeds. As can be seen from this figure, there are no sharp peaks of crystalline
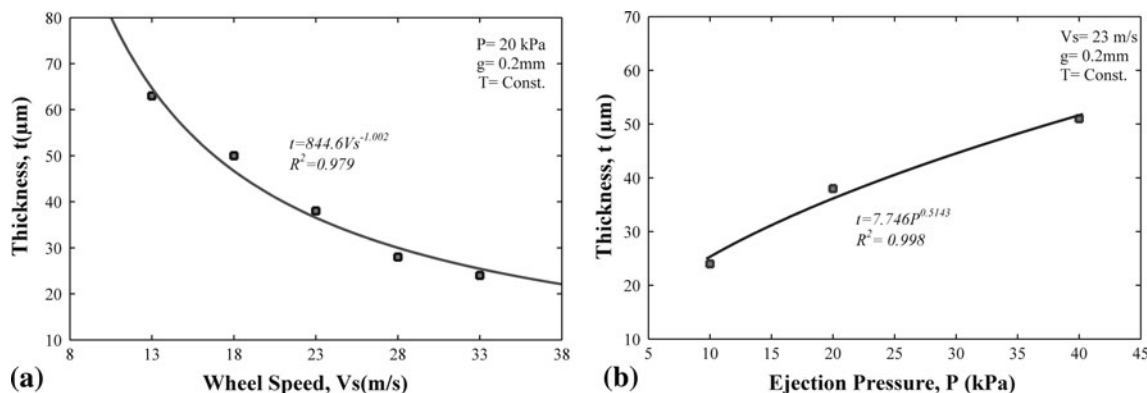

Fig. 1 Variation of thickness with (a) wheel speed and (b) ejection pressure
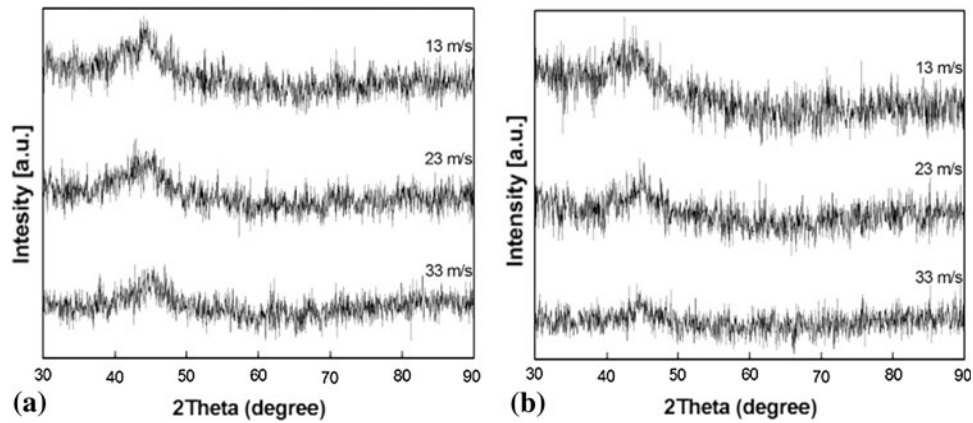
Fig. 2 XRD multiplot patterns of (a) free and (b) contact sides of ribbons produced at wheel speeds of 13, 23, and 33 m/s
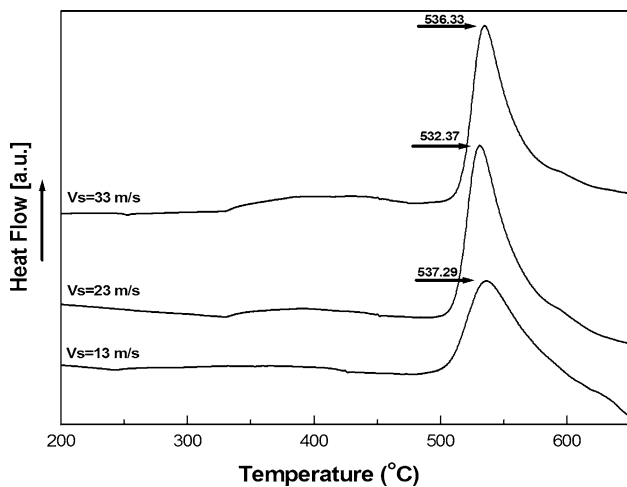

Fig. 3 DSC multiplot of ribbons produced at different wheel speeds (13, 23, and 33 m/s) with a heating rate of 20 K/min

Table 1 Crystallization data for melt spun alloy obtained at different wheel speeds

Vs, m/s	$-\Delta H$, J/g	Tx, °C
13	65.92	507.08
23	70.15	512.79
33	73.08	510.82

T_x crystallization temperature, ΔH enthalpy of crystallization

structure corresponding to bcc-Fe(Si) phase reported for Al/Ge-substituted FINEMET ribbons (Ref 13). Therefore, it could be understood from these figures that the ribbons prepared at different wheel speeds have reached to a fully amorphous structure. Furthermore, for all applied wheel speeds, heat extraction is high enough to cool down the melt at rates more than the critical rate in which a very small fraction (10^{-6}) of liquid could crystallize (Ref 14). The reported critical thickness (the thickness of the ribbon containing a fraction of 10^{-6} of crystallites) for FINEMET-type ribbons produced by the PFC process at similar conditions to this research is 100 μm (Ref 15). Note that variation of thickness for the ribbons produced in the current research occurs in a range (i.e., 63-25 μm) which is lower than the mentioned critical thickness. In addition, it should be mentioned that thinner ribbons should have experienced higher cooling rates than thicker ribbons. The cooling rate strongly depends on the ribbon's thickness and enhances with increasing the wheel speed due to the decrease of the ribbon thickness (Ref 4, 16).

Figure 3 shows the DSC multiplot of ribbons prepared at different wheel speeds. These plots exhibit exothermic peaks which correspond to the crystallization of amorphous phase. The magnitudes of crystallization temperature (Tx) and exothermic crystallization energy drawn from DSC graphs are

listed in Table 1. The data show that crystallization begins at similar values of crystallization temperature (Tx) for all ribbons. Further, temperature values at the apex of each plot are very close to each other (Fig. 3). This behavior has also been observed for FINEMET ribbons in other investigations (Ref 13, 17).

As can be seen from Table 1, the exothermic crystallization energy (i.e., the area under the exothermic peak) of ribbons rises by increasing the wheel speed. This trend provides good evidence that the degree of amorphicity of ribbons increases by applying higher values of wheel speed. Indeed, applying higher wheel speeds raises the value of entrapped energy in the ribbon through increasing the number of defects (such as quenched-in nuclei in groups, excess trapped vacancies, etc.) in the form of clusters of structural free volumes of the amorphous state, which are known as a function of the processing conditions (Ref 17). Greer (Ref 18) has also reported that the rate of nucleation during annealing treatment is proportional to the inverse square of the cooling rate. Thicker ribbons are those being quenched at lower wheel speeds and consequently have undergone lower cooling rates and would be expected to have a higher activation energy of crystallization during annealing.

3.3 Dependence of Surface Quality of Ribbons on the Wheel Speed

Figure 4 shows the surface topography of the wheel side surface of the ribbons produced at three different wheel speeds. For the ribbons processed at low (13 m/s) and moderate (23 m/s) wheel speeds, a wavy pattern is formed on the ribbon surface; however, for the highest applied wheel speed (33 m/s), the produced ribbon exhibits a herringbone pattern (containing

of a series of very fine markings). Apparently, the ribbon produced at the wheel speed of 33 m/s seems to have a smoother surface than the two other ribbons.

Figure 5 shows the results of surface roughness measurements for ribbons' contact and free sides. As can be realized from the graph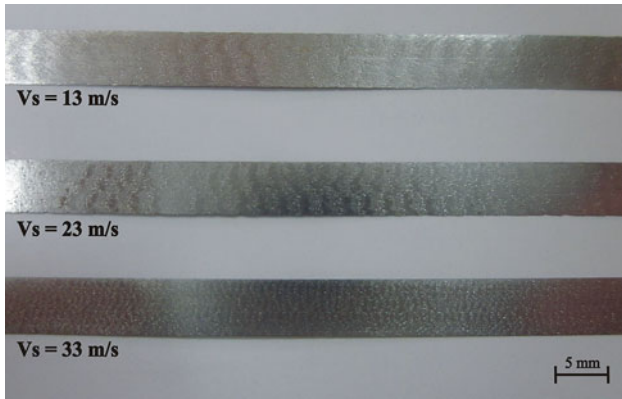, the higher the wheel speed, the lower the surface roughness. Moreover, at a constant wheel speed, values of the measured surface roughness are reduced on the contact side of the ribbons relative to their free side.

Fig. 4 Surface topography of ribbons produced at low (13 m/s), moderate (23 m/s), and high (33 m/s) wheel speeds

Fig. 5 Dependence of Surface roughness (R_a) on the wheel speed for the prepared FINEMET ribbons
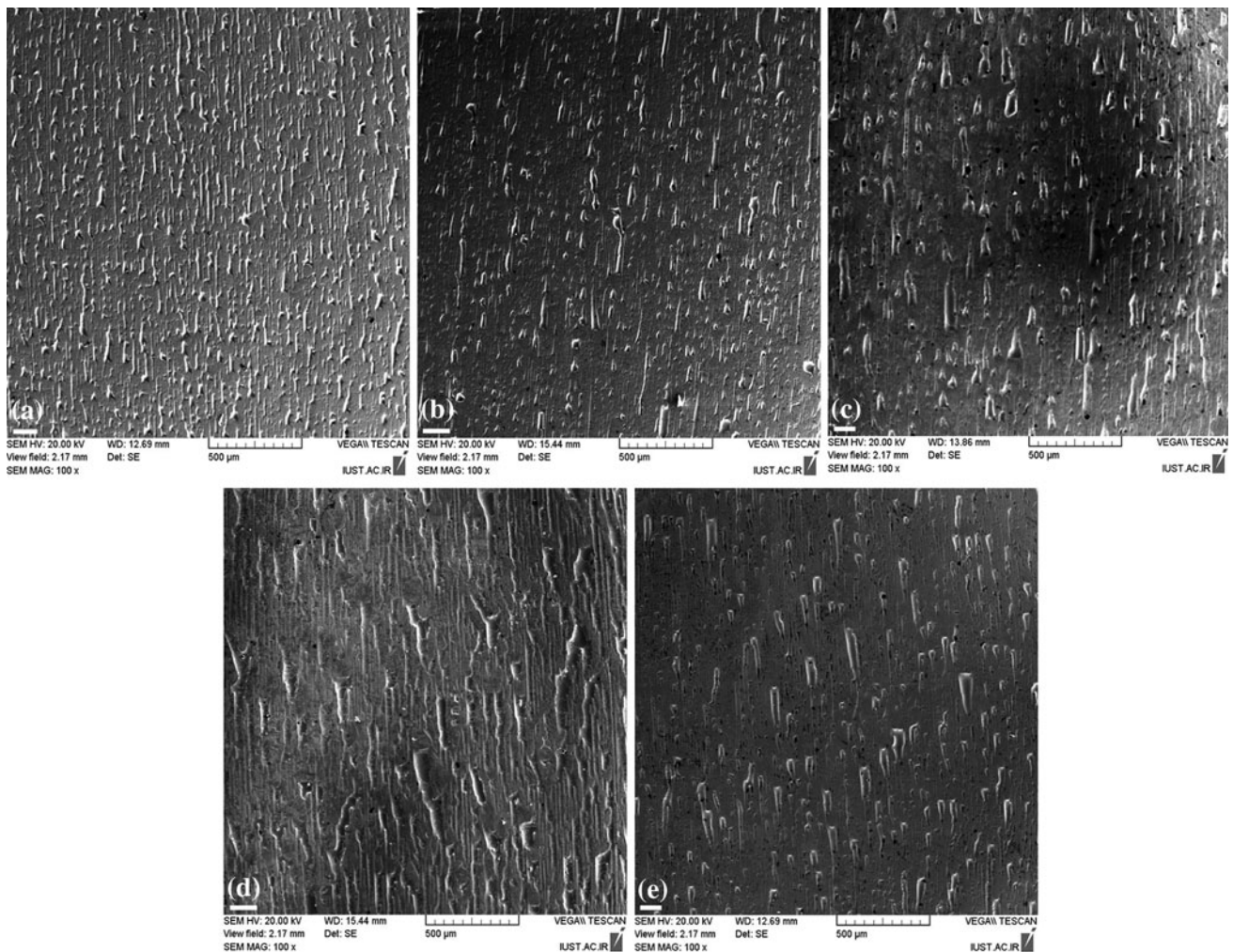

Fig. 6 SEM micrographs of contact side of ribbons prepared at wheel speeds of (a) 13, (b) 18, (c) 23, (d) 28, and (e) 33 m/s

In comparison to data reported for FINEMET ribbons (Ref 15), values of surface roughness measured for FINEMET ribbons in the present study are less than the reported data. On the other hand, the trend of surface roughness reduction with increasing the wheel speed (Fig. 5) contradicts the trend reported for FINEMET alloy. Srinivas et al. (Ref 15) have mentioned that raising the wheel speed increases perturbation in the melt puddle and as a result, roughness of the surface increases. Nonetheless, studies of Napolitano and Meco (Ref 10) on the melt puddle behavior during free jet melt spinning of Fe-Si-B alloy revealed that surface roughness of the ribbons reaches a minimum by applying wheel speeds between 20 and 30 m/s and increases rapidly on the either side of this range.

SEM micrographs of ribbons' contact side may evidence the reducing trend of surface roughness with increasing the wheel speed (Fig. 6). The micrographs exhibit air pocket morphology at the contact interface, which is strongly influenced by the wheel speed. These air pockets seem to be constituted due to the entrapment of air at the wheel-melt interface. Air pockets represent regions of high thermal contact resistance at the wheel-melt interface as a result of poor contact between the ribbon and wheel surface. As can be detected from SEM micrographs, the increase of the wheel speed has reduced the number of air pockets entrapped, and subsequently contact area at the wheel-melt interface has increased. This might be due to the enhancement of heat transfer at the interface by increasing the wheel speed. Several experimental studies have found that the heat transfer coefficient at the wheel-melt contact interface improves by increasing the wheel speed (Ref 19-21). In addition, a numerical study carried out by Sharif and Banerjee (Ref 22) also justifies this argument. Therefore, it can be inferred from the above discussion that an increase in heat transfer coefficient can enlarge the contact area between the melt and the wheel and lower air pockets entrapped at the interface. Consequently, one can expect that surface roughness decreases by increasing the wheel speed, so that the surface quality can be improved.

As illustrated in Fig. 6, the number of air pockets is diminished by increasing the wheel speed. Subsequently, the contact area of liquid at the wheel-melt interface increases and more heat can be extracted by the cooling wheel, which leads to the achievement of higher amounts of cooling rates. Thus, it could be stated that the degree of amorphicity for the ribbons enhances by increasing the wheel speed. This finding is also in line with the results of the DSC graphs (Fig. 3).

4. Conclusions

Amorphous ribbons of $Fe_{71}Si_{13.5}B_9Nb_3Cu_1Al_{1.5}Ge_1$ (at.%) alloy with thicknesses less than 70 μm were fabricated with applying different values of wheel speed and ejection pressure. The main results can be concluded as follows:

1. It was shown that the trend of thickness variation, $t \propto Vs^{-1.08}$ and $t \propto P^{0.514}$, is very close to the predictions of the Bernoulli equation for the PFC process $t \propto Vs^{-1}$ and $t \propto P^{0.5}$).
2. XRD patterns revealed that for applied wheel speeds of 13, 23, and 33 m/s, a fully amorphous structure is achieved since no sharp peaks of crystalline phases exist in the patterns. All produced ribbons are thin enough (63-25 μm) to hinder the formation of crystalline phases.

3. DSC results revealed that applying higher wheel speeds/cooling rates is associated with an increase in the magnitude of enthalpy of crystallization, which correspondingly substantiates improving of the degree of amorphicity with increasing the wheel speed/cooling rate.
4. Evaluation of surface roughness measurements and SEM micrographs revealed that surface roughness decreases by increasing the wheel speed due to reduction of air pockets at the wheel-melt interface and improvement of heat transfer.

References

1. M.C. Narasimhan, United States Patent, No. 4142571, 1979
2. R.W. Cahn, Background to Rapid Solidification Processing, *Rapidly Solidified Alloys: Processes, Structures, Properties, Applications*, H.H. Liebermann, Ed., CRC Press, New York, 1993, p 1–16
3. P.D. Wilde and E.F. Matthys, Experimental Investigation of the Planar Flow Casting Process: Development and Free Surface Characteristics of the Solidification Puddle, *Mater. Sci. Eng. A*, 1992, **150**, p 237–247 (in English)
4. V.I. Tkatch, A.I. Limanovskii, S.N. Denisenko, and S.G. Rassolov, The Effect of the Melt-Spinning Processing Parameters on the Rate of Cooling, *Mater. Sci. Eng. A*, 2002, **323**, p 91–96 (in English)
5. H. Fiedler, H. Muhlbach, and G. Stephani, The Effect of the Main Processing Parameters on the Geometry of Amorphous Metal Ribbons During Planar Flow Casting (PFC), *J. Mater. Sci.*, 1984, **19**, p 3229–3235 (in English)
6. J.K. Carpenter and P.H. Steen, Planar-Flow Spin-Casting of Molten Metals, Process Behavior, *J. Mater. Sci.*, 1992, **27**, p 215–225 (in English)
7. T.J. Praisner, J.S.-J. Chen, and A.A. Tseng, An Experimental Study of Process Behavior in Planar Flow Melt Spinning, *Metall. Mater. Trans. B*, 1995, **26**, p 1199–1208 (in English)
8. C.J. Byrne, A. Theisen, B.L. Reed, and P.H. Steen, Capillary Puddle Vibrations Linked to Casting-Defect Formation in Planar-Flow Melt Spinning, *Metall. Mater. Trans. B*, 2006, **37**, p 445–456 (in English)
9. T. Haga and S. Suzuki, Single Roll Method for Foil Casting of the Aluminum Alloy, *J. Mater. Process. Technol.*, 2003, **137**, p 86–91 (in English)
10. R.E. Napolitano and H. Meco, The Role of Melt Pool Behavior in Free-Jet Melt Spinning, *Metall. Mater. Trans. A*, 2004, **35**, p 1539–1553 (in English)
11. Y. Yoshizawa, S. Oguma, and K. Yamauchi, New Fe-based Soft Magnetic Alloys Composed of Ultrafine Grain Structure, *J. Appl. Phys.*, 1988, **64**(10), p 6044–6046 (in English)
12. F. Shahri, A. Beitollahi, S.G. Shabestari, N. Ghanaatshoar, M.M. Tehranchi, S.M. Mohseni, S.E. Roozmeh, N. Wanderka, and F. Fiorillo, Structural Characterization and Magnetoimpedance Effect in Amorphous and Nanocrystalline AlGe-Substituted FeSiBNbCu Ribbons, *J. Magn. Magn. Mater.*, 2007, **312**, p 35–42 (in English)
13. F. Shahri and A. Beitollahi, Effect of Super-Heat Treatment and Quenching Wheel Speed on the Structure and Magnetic Properties of Fe-Si-Nb-Cu-B-Al-Ge Melt Spun Ribbons, *J. Non Cryst. Solids*, 2008, **354**, p 1487–1493 (in English)
14. D. Turnbull, Under What Conditions Can a Glass be Formed?, *Contemp. Phys.*, 1969, **10**, p 473–488 (in English)
15. M. Srinivas, B. Majumdar, G. Phanikumar, and D. Akhtar, Effect of Planar Flow Melt Spinning Parameters on Ribbon Formation in Soft Magnetic $Fe_{68.5}Si_{18.5}B_9Nb_3Cu_1$ Alloy, *Metall. Mater. Trans. B*, 2011, **42**, p 370–379 (in English)
16. Y.W. Kim, Y.M. Yun, and T.H. Nam, The Effect of the Melt Spinning Processing Parameters on the Solidification Structures in Ti-30 at.% Ni-20 at.% Cu Shape Memory Alloys, *Mater. Sci. Eng. A*, 2006, **438-440**, p 545–548 (in English)
17. M. Srinivas, B. Majumdar, and D. Akhtar, Influence of Wheel Speed During Planar Flow Melt Spinning on the Microstructure and Soft

Magnetic Properties of $Fe_{68.5}Si_{18.5}B_9Nb_3Cu_1$ Ribbons, *J. Mater. Sci.*, 2011, **46**, p 616–622 (in English)

18. A.L. Greer, Crystallisation Kinetics of $Fe_{80}B_{20}$ Glass, *Acta Metall.*, 1982, **30**, p 171–192 (in English)

19. S.C. Huang and H.C. Fiedler, Amorphous Ribbon Formation and the Effects of Casting Velocity, *Mater. Sci. Eng.*, 1981, **51**, p 39–46 (in English)

20. A.G. Gillen and B. Cantor, Photocalorimetric Cooling Rate Measurements on a Ni-5 wt% Al Alloy Rapidly Solidified by Melt Spinning, *Acta Metall.*, 1985, **33**(10), p 1813–1825 (in English)

21. V.I. Tkatch, S.N. Denisenko, and O.N. Beloshov, Direct Measurements of the Cooling Rates in the Single Roller Rapid Solidification Technique, *Acta Mater.*, 1997, **45**(7), p 2821–2826 (in English)

22. M.A.R. Sharif and A. Banerjee, Numerical Analysis of Heat Transfer Due to Confined Slot-Jet Impingement on a Moving Plate, *Appl. Therm. Eng.*, 2009, **29**, p 532–540 (in English)